Nanoscopic Amyloid Pores Formed via Stepwise Protein Assembly

ARTICLE *in* JOURNAL OF PHYSICAL CHEMISTRY LETTERS · JANUARY 2013

Impact Factor: 7.46 · DOI: 10.1021/jz3019786

5 AUTHORS, INCLUDING:

Mily Bhattacharya
Indian Institute of Science Education & Rese…
18 PUBLICATIONS **197** CITATIONS

Neha Jain
Devi Ahilya University, Indore
9 PUBLICATIONS **115** CITATIONS

Soumyadyuti Samai
University of Washington Seattle
3 PUBLICATIONS **3** CITATIONS

Samrat Mukhopadhyay
Indian Institute of Science Education & Rese…
34 PUBLICATIONS **1,054** CITATIONS

THE JOURNAL OF PHYSICAL CHEMISTRY Letters

Letter

pubs.acs.org/JPCL

Nanoscopic Amyloid Pores Formed via Stepwise Protein Assembly

Mily Bhattacharya,*[,†,§] Neha Jain,[‡,§] Priyanka Dogra,[†] Soumyadyuti Samai,[†] and Samrat Mukhopadhyay*[,†,‡]

[†]Department of Chemical Sciences and [‡]Department of Biological Sciences, Indian Institute of Science Education and Research (IISER), Mohali, Knowledge City, Sector 81, S.A.S. Nagar, Mohali-140306, India

Supporting Information

ABSTRACT: Protein aggregation leading to various nanoscale assemblies is under scrutiny due to its implications in a broad range of human diseases. In the present study, we have used ovalbumin, a model non-inhibitory serpin, to elucidate the molecular events involved in amyloid assembly using a diverse array of spectroscopic and imaging tools such as fluorescence, laser Raman, circular dichroism spectroscopy, and atomic force microscopy (AFM). The AFM images revealed a progressive morphological transition from spherical oligomers to nanoscopic annular pores that further served as templates for higher-order supramolecular assembly into larger amyloid pores. Raman spectroscopic investigations illuminated in-depth molecular details into the secondary structural changes of the protein during amyloid assembly and pore formation. Additionally, Raman measurements indicated the presence of antiparallel β-sheets in the amyloid core. Overall, our studies revealed that the protein conformational switch in the context of the oligomers triggers the hierarchical assembly into nanoscopic amyloid pores. Our results will have broad implications in the structural characterization of amyloid pores derived from a variety of disease-related proteins.

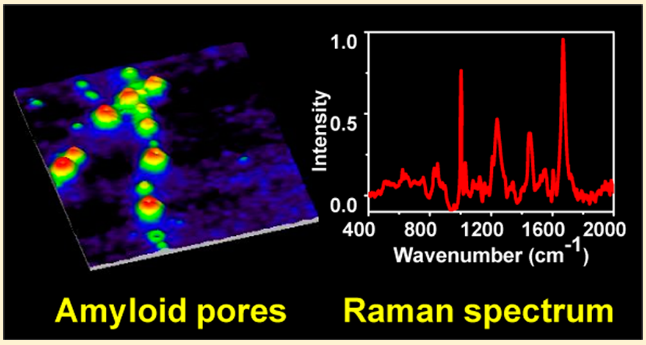

SECTION: Biophysical Chemistry and Biomolecules

The phenomenon of self-assembly of simpler subunits leading to exotic supramolecular assemblies is ubiquitous in many chemical and biological systems;[1] however, uncontrolled self-association of the precursor units, for example, proteins, might lead to adverse consequences. For instance, an enormous number of human diseases are identified to be protein conformational disorders that originate from the uncontrolled self-assembly and deposition of misfolded protein aggregates and amyloids.[2−9] These disorders are manifested in a range of neurodegenerative diseases like Alzheimer's, Parkinson's, and so on as well as in systemic amyloidoses and serpinopathies. Serpinopathies are described as a range of physiological diseases that occur as a consequence of misfolding and self-assembly of serpins (serine protease inhibitors), such as neuroserpin and α-antitrypsin, which lead to Alzheimer-like dementia, liver cirrhosis, and hepatocellular carcinoma, respectively.[10,11] Both the wild-type and mutants of archetypal serpins have been shown to aggregate.[12−15] Although two major different ways of serpin polymerization have been proposed,[12−17] the mechanism of serpin self-assembly still remains elusive.

Ovalbumin, a 385-residue, 45 kDa glycoprotein (Figure 1A), is a model non-inhibitory member of the serpin superfamily that is present in the chicken egg-white and is commonly used as a gelling agent, emulsifier, and so on in the food industry.[18−20] The structural similarity between ovalbumin and other archetypal serpins (α-antitrypsin, neuroserpin) coupled to the ease of availability renders ovalbumin an attractive candidate for investigating the mechanistic aspects of serpinopathies. Several reports have demonstrated that the native and the acid-induced molten-globule state of ovalbumin undergo irreversible aggregation at an elevated temperature involving a profound conformational change from largely α-helical to β-sheet-rich structure.[21−25] However, the mechanism of amyloid aggregation as well as the organization of individual protein molecules within the supramolecular amyloid assembly are poorly understood.

In addition to the quest of a comprehensive molecular mechanism of amyloid formation, there is a pressing need to delineate the cascade of molecular events during protein self-assembly coupled to cytotoxicity. An increasing body of evidence suggests that the oligomeric or prefibrillar intermediates are more cytotoxic compared with the matured amyloid fibrils.[26,27] Among various oligomeric structures, annular pore-based morphology is also commonly observed.[27] Several hypotheses suggest that amyloid pores permeabilize cell membranes by a mechanism, conjectured to be similar to that of pore-forming bacterial toxins,[26] although other types of membrane disruption mechanisms are also proposed to be

Received: November 29, 2012
Accepted: January 22, 2013

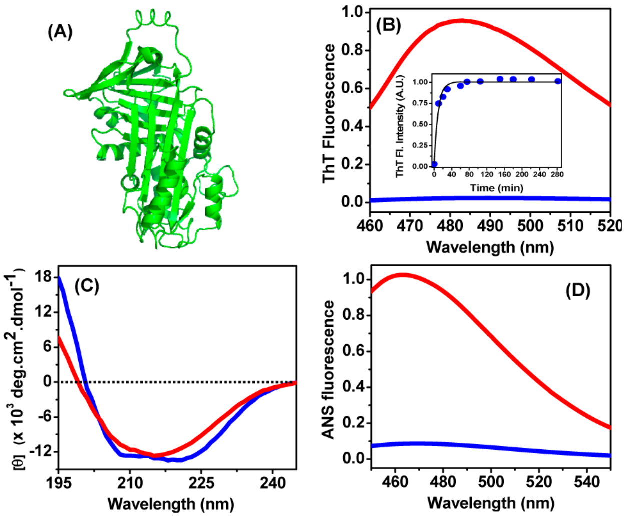

Figure 1. (A) Crystal structure of ovalbumin (PDB ID: 1OVA) generated using PyMol (DeLano Scientific, CA). Changes in the (B) ThT fluorescence (inset shows the ThT fluorescence kinetics), (C) far-UV CD spectra, and (D) ANS fluorescence during amyloid aggregation. The blue and the red solid lines represent the spectra of protein samples before and after incubation (4 h at 65 °C), respectively. The fluorescence spectra are intensity-normalized, and the solid line in the inset graph represents the single-exponential fit that was used to recover the apparent rate constant.

quite effective in causing neurodegeneration.[27] However, molecular insights into the transition of a soluble monomeric protein into donut-shaped supramolecular amyloid pores leading to nanoscopic amyloid assemblies are quite limited. In the present study, we have used a combination of Raman spectroscopy and atomic force microscopy (AFM) imaging that provided in-depth insights into both molecular and nanoscale structural changes of ovalbumin during stepwise morphological transformation of the soluble precursor into amyloid annular pores. Additionally, we have been able to elucidate the hierarchical structural arrangement of protein molecules within the supramolecular annular assemblies.

We have previously reported that the monomeric ovalbumin forms a partially unfolded molten-globule state at low pH.[28] This prompted us to investigate whether the molten-globule state can form amyloid aggregates in vitro under suitable conditions. The aggregation reaction was monitored by the changes in the fluorescence of a well-known amyloid-reporter, Thioflavin-T (ThT), and circular dichroism (CD) spectroscopy. A 30-fold increase in the ThT fluorescence (Figure 1B) compared with the sample before incubation indicated the formation of cross β-structured amyloid aggregates with an apparent rate constant of $(114 \pm 6) \times 10^{-3}$ min^{-1} (Figure 1B inset). Similarly, far-UV CD measurements indicated a conformational transformation from a predominantly α-helical molten-globule precursor to β-sheet-rich aggregates (Figure 1C). Also, a sharp increase in the fluorescence intensity of ANS (8-anilinonaphthalene-1-sulfonic acid), a well-known environment-sensitive fluorescent dye,[29] suggested that amyloid formation was predominantly driven by hydrophobic association in addition to electrostatic interactions (Figure 1D).

After establishing that ovalbumin indeed forms amyloid aggregates, the morphological transformations were investigated as a function of time using AFM that also provided insights into the time-dependent evolution of the topography of the supramolecular nanoscale assemblies. Before the sample was incubated, spherical oligomeric aggregates were observed

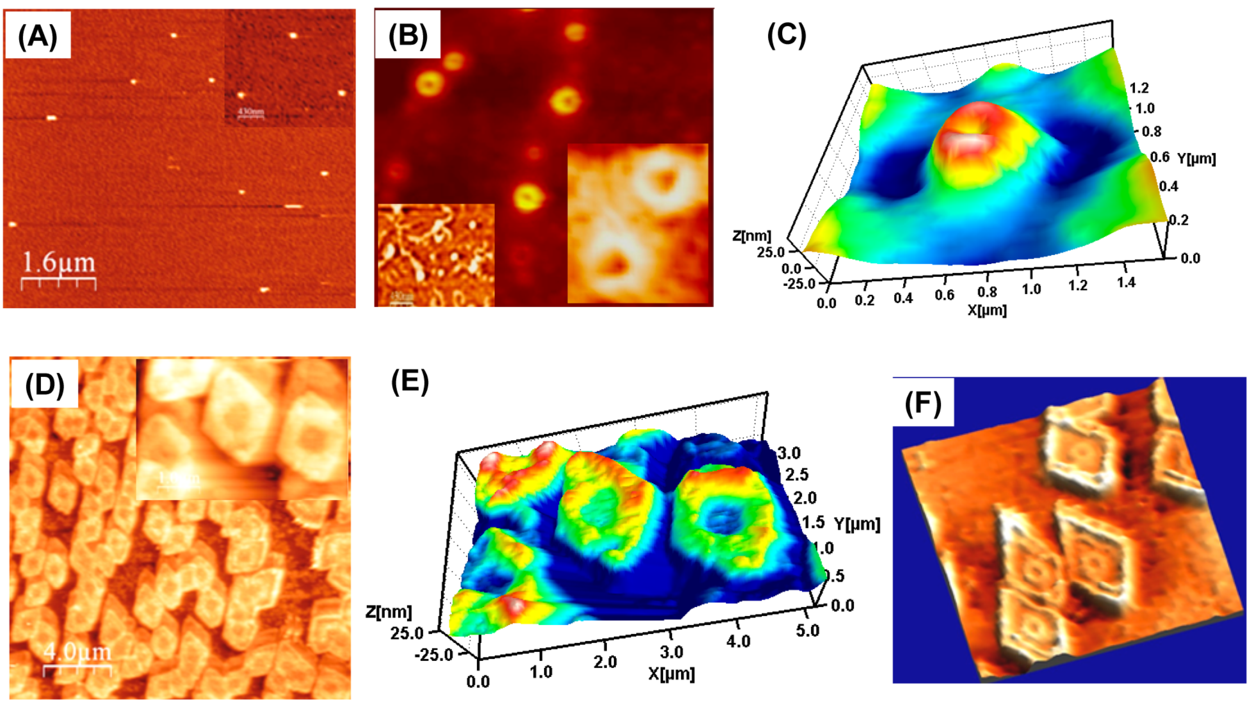

Figure 2. AFM images of ovalbumin (A) soluble oligomers formed at room temperature (scale bar: 1.6 μm) (inset shows an expanded view of a few oligomers), (B) annular pores after 15 min of incubation at 65 °C (scale bar: 1.4 μm) (insets show expanded views of both worm-like fibrils (left) and annular pores (right)), (C) 3D representation of a single amyloid pore, (D) higher order, supramolecular annular pores after 4 h of incubation (scale bar: 4 μm) (inset shows an expanded view of the larger pores), (E) 3D representation of the large pores, and (F) amyloid pores formed after 24 h (incubated at room temperature after 4 h of heating at 65 °C; scale bar: 3 μm).

dx.doi.org/10.1021/jz3019786 | J. Phys. Chem. Lett. 2013, 4, 480−485

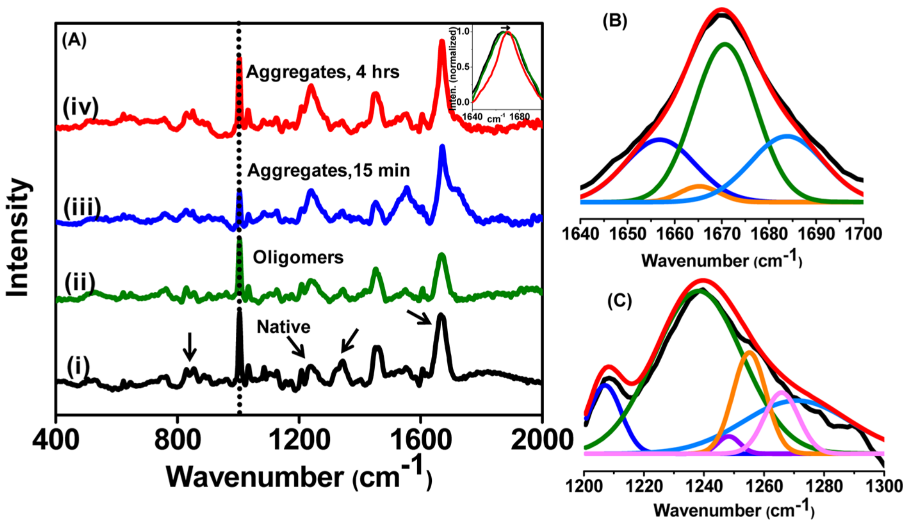

Figure 3. (A) Solution Raman spectra of ovalbumin in the (i) native form (black solid line) at pH 7 and (ii–iv) aggregates formed at pH 2.2 (green, blue, and red solid lines for 0 min, 15 min, and 4 h, respectively) at an excitation wavelength of 514 nm. The black short-dotted line is the Raman peak at 1003 cm^{-1} due to phenylalanine (internal standard) present in ovalbumin and the black arrows denote specific Raman spectral regions: Tyrosine Fermi doublet (829 and 855 cm^{-1}), amide III (1230–1300 cm^{-1}), tryptophan Fermi doublet (1340 and 1360 cm^{-1}), and amide I (1640–1690 cm^{-1}). Inset graph shows the shift of amide I band from 1666 to 1670 cm^{-1} (depicted by an arrow) indicating the evolution of cross β-sheet structure during ovalbumin amyloid assembly. All of the Raman spectra in the inset are intensity-normalized at the respective peak maximum. Gaussian deconvolution of the (B) amide I and (C) amide III regions, collected after 4 h of incubation, to analyze the percentage composition of various secondary structures. The black and the red solid lines in (B,C) represent the actual data and the cumulative fit, respectively. The other colored solid lines (dark blue: α-helix; green: β-sheet; orange: random coil; sky blue: extended structure) represent the Gaussian peaks obtained after deconvolutions.

and statistical analyses revealed a narrow unimodal height distribution centered at ~3.5 nm (Figure 2A and Figures S1 and S2A,B of the Supporting Information). Upon thermal incubation, the nanoscale morphology of the sample (after 15 min) showed a heterogeneous distribution predominated by the presence of annular pore-like aggregates in addition to worm-like structures (Figure 2B). For visual clarity, a 3D representation of one of the donut-shaped pores is shown in Figure 2C. The height distribution profiles (Figure S2C,D of the Supporting Information) as well as statistical analyses (Figure S2E of the Supporting Information) revealed that the annular pore topography ranged between 20 and 40 nm, whereas that of the less-populated, worm-like structures varied from 10 to 15 nm. The average diameter of the pores was ~50 nm (54 ± 9 nm). Upon prolonged incubation, the proportion and the dimensions of these annular pores increased further (Figure 2D,E), and the topographical distribution reflected an average height of ~50–60 nm, whereas the proportion of aggregates with height of ~10 nm reduced by ~50% (Figure S3A,B of the Supporting Information). These annular pores share morphological resemblance with the "beads-on-a-string" morphology[12,13,30] described for α-antitrypsin aggregates but are in contrast with a few reports where electron micrographs of ovalbumin aggregates reveal semiflexible or rod-like fibrils along with amorphous aggregates.[21,22,24] Given that a variety of amyloidogenic peptides and globular as well as intrinsically disordered proteins have been shown to form annular pores and protofibrils in vitro as a function of pH, ionic strength, and metal ion concentration,[31−37] the formation of annular species is conjectured to be a generic phenomenon because they are formed irrespective of a protein being disease-related or not. Interestingly after 24 h, the aggregate morphology showed an array of concentric aggregates wherein each annular pore was encircled by twisted aggregates (Figure 2F) and the respective height distribution histogram depicted an average height of 60–70 nm (Figure S3C of the Supporting Information). Hence, investigation of the overall assembly process revealed that the spherical oligomers, formed at room temperature, associated to form both small annular pores and worm-like fibrils (upon heating). The annular pores were then utilized as scaffolds by the worm-like aggregates that intertwined around these pores and triggered the hierarchical nanoscale assembly in a stepwise manner into higher-order supramolecular amyloid pores that remained soluble even for several days. This templated-assembly of annular pores is supported by the height distribution histogram that showed a decrease in the aggregate population of height ~10 nm with a simultaneous increase in the height of 50–70 nm. However, we do not rule out the possibility of dissociation of the worm-like aggregates into smaller oligomers that subsequently reassociate with preformed pores leading to higher order assembly.

Next, efforts were steered toward delineating the protein structural changes of the nanoscopic amyloid pores at the molecular level by Raman spectroscopy that provides a wealth of information about both the polypeptide backbone and the amino acid residues involved in aggregation.[38,39] The backbone amide group markers such as amide I and amide III regions as well as a few aromatic side-chain markers such as tryptophans and tyrosines were monitored carefully and subsequently analyzed to probe the changes (and/or shift) in the respective band positions and intensities as a function of aggregation. Both the amide regions denote the presence of secondary structural elements such as α-helix, β-sheet, and random coils. More importantly, these regions also provide information about (i) whether the β-sheet is parallel or antiparallel and (ii) whether the cross-β-sheet-rich structure at 1670 cm^{-1}, a potent hallmark of amyloid fibril formation, evolves as a function of aggregation.[38,39] Figure 3Ai shows the Raman spectrum of the native ovalbumin, which corroborated well with that previously reported.[40,41] Deconvolution of the spectrum followed by percentage analysis yielded the secondary structural contents that agreed well with that extracted from the respective CD spectrum.[28] Analysis of the amide I and III regions of the oligomeric species, formed at room temperature (Figure 3Aii), indicated a small but significant decrease in the α-helical content with a concomitant increase in the random-coil content as expected (Tables S1 and S2 of the Supporting Information). Following this observation, the sample was incubated at 65 °C to trigger the aggregation. Figure 3Aiii,iv shows the representative solution Raman spectra of amyloid aggregates obtained after 15 min and 4 h of incubation, respectively. A careful look at all spectra revealed that upon incubation the peak maximum of the amide I band shifted from 1666 (observed in both the native and molten-globule-oligomers of ovalbumin) to 1670 cm^{-1}, suggestive of the formation of cross-β-sheet-rich amyloid aggregates as a function of time (Figure 3A inset) similar to that observed for insulin and β_2-microglobulin amyloid fibrils.[42,43] Also, the amide I band that was initially broad became sharper after 4 h of incubation. Deconvolution (Figure 3B) and percentage analysis of the amide I region suggested a decrease in both the α-helical (reduced further) and random-coil contents in the amyloid aggregates as compared with the spherical oligomers (Table S1; Supporting Information). On the contrary, the β-sheet content increased upon incubation as aggregation progressed, thus supporting the evolution of Raman band at 1670 cm^{-1}. Next, similar careful consideration was given for the amide III Raman band analysis. The amide III band, which appeared broad initially, became sharper during the course of aggregation, similar to that observed for the amide I band. Analysis of the amide III region (Figure 3C) corroborated the same trend; an increase in β-sheet content was observed, whereas both the α-helical and random-coil contents decreased (Table S2; Supporting Information). Additionally, the band at 1240 cm^{-1} gained prominence and became sharper, indicating the rearrangement of β-strands into antiparallel β-sheets similar to that observed in heat-denatured ovalbumin aggregates at pH 7[41] and insulin filaments.[44] Therefore, combining the results obtained from the analyses of amide I and III regions, we propose that the ovalbumin aggregation proceeds via loss in the α-helical content with a concomitant increase in random-coil structure, which eventually leads to the formation of cross-β-sheet-rich amyloid pores that constitute antiparallel β-sheets in the amyloid core. Additionally, the value of Ramachandran ψ dihedral angle of the amyloid pores could be estimated from the amide III Raman band (at 1240 cm^{-1}) representing the antiparallel β-sheets.[45,46] Using an empirical relationship,[47] the average Ramachandran ψ dihedral angle was determined to be ~+135°, which agrees well with the results obtained for amyloid fibrils derived from Alzheimer's Aβ peptide.[45]

After the backbone conformational analysis, the changes in the environment around the aromatic side-chain markers such as tyrosines and tryptophans as a consequence of aggregation were also investigated. The ratio of intensities at 850 to 830 cm^{-1} (tyrosine Fermi doublet),[38,39] denoted as I_{850}/I_{830}, serves as an indicator of the hydrogen bonding strength between the phenolic hydroxyl moiety (of tyrosine) and the solvent molecules.[39,48] In our case, we observed the tyrosine doublet at 829 and 855 cm^{-1} at all aggregation stages of ovalbumin. Ratio analysis (I_{855}/I_{829}) followed by a comparison suggested that the hydrogen bonding strength between the phenolic hydroxyl and the surrounding water molecules varied from strong (1.7 in the native) to moderate (1.0 in the aggregated species). However, we must emphasize that the nature of hydrogen bonding mentioned here is an average estimate because ovalbumin contains ten tyrosines.[48] We can only infer that the tyrosines became partially buried and formed transient hydrogen bonds with the aqueous surroundings[49] as aggregation progressed, which was reflected in the diminution of the average hydrogen bonding strength. Similarly, tryptophan also exhibits the Fermi doublet at 1340 and 1360 cm^{-1}.[37,39] The ratio of band intensities at 1360 to 1340 denoted as I_{1360}/I_{1340} is a measure of strong hydrophobic interactions between the indole ring (of tryptophan) and the neighboring aliphatic groups.[50,51] In our study, we observed a continuous increase in the I_{1360}/I_{1340} ratio, as we moved from the native (0.3) to the aggregated states (1.0), implying an increase in the average hydrophobicity of the environment around the tryptophans. Similar sequestration of tryptophans has been commonly observed in the amyloid fibrils formed from other globular proteins.[43] Here again we mention an average hydrophobic environment because ovalbumin contains three tryptophan residues. Additionally, tryptophan exhibits another Raman band at 880 cm^{-1} that is assigned to the hydrogen bonding strength between the −N−H of the indole ring and the surrounding solvent molecules.[39] It has been shown that this band at 880 cm^{-1} shifts to 871 cm^{-1} if the hydrogen bonding is quite strong, whereas a lack of any hydrogen bond shifts the band to 883 cm^{-1}.[39,51,52] For native ovalbumin, the band appeared at 877 cm^{-1} indicative of moderately strong hydrogen bonds, which is in accordance with its crystal structure.[18] The oligomeric species revealed two bands at 877 and 886 cm^{-1}, suggesting that at least one of the three tryptophans forms moderately strong hydrogen bonds with its neighboring water molecules.[52] Interestingly, both the aggregated species formed after 15 min and 4 h of incubation exhibited Raman band at 881 cm^{-1}, thus indicating the absence of any hydrogen bonds. This also implied that the tryptophans get progressively buried, which renders the indole group inaccessible to form hydrogen bonds with the water molecules, hence corroborating the results obtained from the I_{1360}/I_{1340} ratio. Taken together, our Raman spectroscopic studies suggest that a gradual sequestration of tryptophans and tyrosines into the amyloid core ensued as a consequence of a conformational switch from α-helical to cross-β structured amyloid pores.

In summary, we have demonstrated that the predominantly α-helical molten-globule state of ovalbumin undergoes a profound conformational rearrangement, presumably by a previously described mechanism,[53] and self-associates in a stepwise manner to form cross β-rich amyloid pores with an average diameter of ~50 nm. These nanoscopic pores further serve as templates for the genesis of higher order supramolecular pores. Additionally, detailed structural information obtained from Raman spectroscopy revealed a progressive sequestration of tryptophans and tyrosines into the amyloid pores consisting of antiparallel β-sheets in the core. We believe that the structural insights gained from this study will help in the design of anti-amyloid therapeutics targeted toward combating serpin self-assembly and other devastating amyloid disorders. Additionally, because these amyloid pores are exotic soft nanoporous materials, we envision that the conformational control of this fascinating class of supramolecular protein assembly would find broad applications in the design of advanced functional bionanomaterials.[8]

■ EXPERIMENTAL SECTION

For aggregation experiments, ovalbumin stock (pH 7, 5 mM) was diluted 10-fold into pH 2.2 (50 mM, Gly-HCl buffer) containing 50 mM NaCl to a final protein concentration of 100 μM. The resulting protein sample was then heated to 65 ± 1 °C using a heating block that was already preset at the required temperature under quiescent condition. The AFM images of the ovalbumin aggregates were collected on a Multiview^{2000} scanning probe microscope (Nanonics Imaging, Israel), and the solution Raman spectra were collected on an inVia Raman microscope (Renishaw, U.K.) at ~24 °C. For all experimental and data analyses details, please see the Supporting Information.

■ ASSOCIATED CONTENT

Ⓢ Supporting Information

Experimental and data analyses details along with additional figures. This material is available free of charge via the Internet at http://pubs.acs.org.

■ AUTHOR INFORMATION

Corresponding Author

*E-mail: mily@iisermohali.ac.in; mukhopadhyay@iisermohali.ac.in.

Author Contributions

[§]These authors contributed equally to this work.

Notes

The authors declare no competing financial interest.

■ ACKNOWLEDGMENTS

We thank the members of the Mukhopadhyay lab for reading the manuscript critically. M.B. thanks the Department of Science & Technology (DST), New Delhi for the Women Scientists' grant. S.M. thanks the Council of Scientific & Industrial Research (CSIR), New Delhi for a research grant. P.D. thanks DST for the INSPIRE fellowship, and S.S. thanks the Indian Academy of Sciences, Bangalore for summer research fellowship.

■ REFERENCES

(1) Lehn, J.-M. *Supramolecular Chemistry: Concepts and Perspectives*; Wiley-VCH: Weinheim, Germany, 1995.

(2) Eisenberg, D.; Jucker, M. The Amyloid State of Proteins in Human Diseases. *Cell* **2012**, *148*, 1188−1203.

(3) Adamcik, J.; Mezzenga, R. Proteins Fibrils from a Polymer Physics Perspective. *Macromolecules* **2012**, *45*, 1137−1150.

(4) Lee, J.; Culyba, E. K.; Powers, E. T.; Kelly, J. W. Amyloid-β Forms Fibrils by Nucleated Conformational Conversion of Oligomers. *Nat. Chem. Biol.* **2011**, *7*, 602−609.

(5) Luheshi, L. M.; Crowther, D. C.; Dobson, C. M. Protein Misfolding and Disease: From the Test Tube to the Organism. *Curr. Opin. Chem. Biol.* **2008**, *12*, 25−31.

(6) Jahn, T. R.; Radford, S. E. Folding versus Aggregation: Polypeptide Conformations on Competing Pathways. *Arch. Biochem. Biophys.* **2008**, *469*, 100−117.

(7) *Protein Misfolding, Aggregation and Conformational Diseases: I. Protein Aggregation and Conformational Disorders*; Uversky, V. N., Fink, A. L., Eds.; Springer: New York, 2006.

(8) Cherny, I.; Gazit, E. Amyloids: Not Only Pathological Agents but Also Ordered Nanomaterials. *Angew. Chem. Int. Ed.* **2008**, *47*, 4062−4069.

(9) Dalal, V.; Bhattacharya, M.; Narang, D.; Sharma, P. K.; Mukhopadhyay, S. Nanoscale Fluorescence Imaging of Single Amyloid Fibrils. *J. Phys. Chem. Lett.* **2012**, *3*, 1783−1787.

(10) Gooptu, B.; Lomas, D. A. Conformational Pathology of the Serpins: Themes, Variations and Therapeutic Strategies. *Annu. Rev. Biochem.* **2009**, *78*, 147−176.

(11) Knaupp, A. S.; Bottomley, S. P. Serpin Polymerization and Its Role in Disease-the Molecular Basis of α1-Antitrypsin Deficiency. *IUBMB Life* **2009**, *61*, 1−5.

(12) Lomas, D. A.; Evans, D. L.; Finch, J. T.; Carrell, R. W. The Mechanism of Z α_1-Antitrypsin Accumulation in the Liver. *Nature* **1992**, *357*, 605−607.

(13) Dafforn, T. R.; Mahadeva, R.; Elliott, P. R.; Sivasothy, P.; Lomas, D. A. A Kinetic Mechanism for the Polymerization of α1-Antitrypsin. *J. Biol. Chem.* **1999**, *274*, 9548−9555.

(14) Tsutsui, Y.; Kuri, B.; Sengupta, T.; Wintrode, P. L. The Structural Basis of Serpin Polymerization Studied by Hydrogen/Deuterium Exchange and Mass Spectrometry. *J. Biol. Chem.* **2008**, *283*, 30804−30811.

(15) Ekeowa, U. I.; Freeke, J.; Miranda, E.; Gooptu, B.; Bush, M. F.; Pérez, J.; Teckman, J.; Robinson, C. V.; Lomas, D. A. Defining the Mechanism of Polymerization in the Serpinopathies. *Proc. Natl. Acad. Sci. U.S.A.* **2010**, *107*, 17146−17151.

(16) Yamasaki, M.; Li, W.; Johnson, D. J. D.; Huntington, J. A. Crystal Structure of a Stable Dimer Reveals the Molecular Basis of Serpin Polymerization. *Nature* **2008**, *455*, 1255−1258.

(17) Yamasaki, M.; Sendall, T. J.; Pearce, M. C.; Whisstock, J. C.; Huntington, J. A. Molecular Basis of α1-Antitrypsin Deficiency Revealed by the Structure of a Domain-Swapped Trimer. *EMBO Rep.* **2011**, *12*, 1011−1017.

(18) Stein, P. E.; Leslie, A. G. W.; Finch, J. T.; Carrell, R. W. Crystal Structure of Uncleaved Ovalbumin at l.95 Å Resolution. *J. Mol. Biol.* **1991**, *221*, 941−959.

(19) Donnell, E.R.-O. The Ovalbumin Family of Serpin Proteins. *FEBS Lett.* **1993**, *315*, 105−108.

(20) Mine, Y. Recent Advances in the Understanding of Egg White Protein Functionality. *Trends Food Sci. Technol.* **1995**, *6*, 225−232.

(21) Azakami, H.; Mukai, A.; Kato, A. Role of Amyloid Type Cross β-Structure in the Formation of Soluble Aggregate and Gel in Heat-Induced Ovalbumin. *J. Agric. Food Chem.* **2005**, *53*, 1254−1257.

(22) Pearce, F. G.; Mackintosh, S. H.; Gerrard, J. A. Formation of Amyloid-Like Fibrils by Ovalbumin and Related Proteins under Conditions Relevant to Food Processing. *J. Agric. Food Chem.* **2007**, *55*, 318−322.

(23) Tanaka, N.; Morimoto, Y.; Noguchi, Y.; Tada, T.; Waku, T.; Kunugi, S.; Morii, T.; Lee, Y.-F.; Konno, T.; Takahashi, N. The Mechanism of Fibril Formation of a Non-Inhibitory Serpin Ovalbumin Revealed by the Identification of Amyloidogenic Core Regions. *J. Biol. Chem.* **2011**, *286*, 5884−5894.

(24) Veerman, C.; de Schiffart, G.; Sagis, L. M. C.; van der Linden, E. Irreversible Self-Assembly of Ovalbumin into Fibrils and the Resulting Network Rheology. *Intl. J. Biol. Macromol.* **2003**, *33*, 121−127.

(25) Naeem, A.; Khan, T. A.; Muzaffar, M.; Ahmad, S.; Saleemuddin, M. A Partially Folded State of Ovalbumin at Low pH Tends to Aggregate. *Cell Biochem. Biophys.* **2011**, *59*, 29−38.

(26) Lashuel, H. A.; Lansbury, P. T., Jr. Are Amyloid Diseases Caused by Protein Aggregates That Mimic Bacterial Pore-Forming Toxins? *Q. Rev. Biophys.* **2006**, *39*, 167−201.

(27) Butterfield, S. M.; Lashuel, H. A. Amyloidogenic Protein-Membrane Interactions: Mechanistic Insight from Model Systems. *Angew. Chem. Int. Ed.* **2010**, *49*, 5628−5654.

(28) Bhattacharya, M.; Mukhopadhyay, S. Structural and Dynamical Insights into the Molten-Globule Form of Ovalbumin. *J. Phys. Chem. B* **2012**, *116*, 520−531.

(29) Hawe, A.; Sutter, M.; Jiskoot, W. Extrinsic Fluorescent Dyes As Tools for Protein Characterization. *Pharm. Res.* **2008**, *25*, 1487−1499.

(30) Lomas, D. A.; Finch, J. T.; Seyama, K.; Nukiwa, T.; Carrell, R. W. α_1-Antitrypsin S_{iiyama} (Ser^{53}→ Phe). *J. Biol. Chem.* **1993**, *268*, 15333−15335.

(31) Mališauskas, M.; Zamotin, V.; Jass, J.; Noppe, W.; Dobson, C. M.; Morozova-Roche, L. A. Amyloid Protofilaments from the Calcium-Binding Protein Equine Lysozyme: Formation of Ring and Linear

Structures Depends on pH and Metal Ion Concentration. *J. Mol. Biol.* **2003**, *330*, 879−890.

(32) Zhu, M.; Han, S.; Zhou, F.; Carter, S. A.; Fink, A. L. Annular Oligomeric Amyloid Intermediates Observed by in Situ Atomic Force Microscopy. *J. Biol. Chem.* **2004**, *279*, 24452−24459.

(33) Ghodke, S.; Nielsen, S. B.; Christiansen, G.; Hjuler, H. A.; Flink, J.; Otzen, D. Mapping out the Multistage Fibrillation of Glucagon. *FEBS J.* **2012**, *279*, 752−765.

(34) Capone, R.; Jang, H.; Kotler, S. A.; Kagan, B. L.; Nussinov, R.; Lal, R. Probing Structural Features of Alzheimer's Amyloid-β Pores in Bilayers Using Site-Specific Amino Acid Substitutions. *Biochemistry* **2012**, *51*, 776−785.

(35) Kagan, B. L.; Jang, H.; Capone, R.; Arce, F. T.; Ramachandran, S.; Lal, R.; Nussinov, R. Antimicrobial Properties of Amyloid Peptides. *Mol. Pharmaceutics* **2012**, *9*, 708−717.

(36) Capone, R.; Mustata, M.; Jang, H.; Arce, F. T.; Nussinov, R.; Lal, R. Antimicrobial Protegrin-1 Forms Ion Channels: Molecular Dynamic Simulation, Atomic Force Microscopy, and Electrical Conductance Studies. *Biophys. J.* **2010**, *98*, 2644−2652.

(37) Mukhopadhyay, S.; Nayak, P. K.; Udgaonkar, J. B.; Krishnamoorthy, G. Characterization of the Formation of Amyloid Protofibrils from Barstar by Mapping Residue-Specific Fluorescence Dynamics. *J. Mol. Biol.* **2006**, *358*, 935−942.

(38) Tuma, R. Raman Spectroscopy of Proteins: From Peptides to Large Assemblies. *J. Raman Spectrosc.* **2005**, *36*, 307−319.

(39) Něměček, D.; Thomas, G. J., Jr. In *Handbook Of Molecular Biophysics*; Bohr, H. G., Ed.; Wiley-VCH: Weinhem, Germany, 2009.

(40) Koenig, J. L.; Frushour, B. G. Raman Scattering of Chymotrypsinogen A, Ribonuclease, And Ovalbumin in the Aqueous Solution and Solid State. *Biopolymers* **1972**, *11*, 2505−2520.

(41) Painter, P. C.; Koenig, J. L. Raman Spectroscopic Study of the Proteins of Egg White. *Biopolymers* **1976**, *15*, 2155−2166.

(42) Huang, K.; Maiti, N. C.; Phillips, N. B.; Carey, P. R.; Weiss, M. A. Structure-Specific Effects of Protein Topology on Cross-β Assembly: Studies of Insulin Fibrillation. *Biochemistry* **2006**, *45*, 10278−10293.

(43) Hiramatsu, H.; Lu, M.; Matsuo, K.; Gekko, K.; Goto, Y.; Kitagawa, T. Differences in the Molecular Structure of β_2-Microglobulin between Two Morphologically Different Amyloid Fibrils. *Biochemistry* **2010**, *49*, 742−751.

(44) Zako, T.; Sakono, M.; Hashimoto, N.; Ihara, M.; Maeda, M. Bovine Insulin Filaments Induced by Reducing Disulfide Bonds Show a Different Morphology, Secondary Structure, And Cell Toxicity from Intact Insulin Amyloid Fibrils. *Biophys. J.* **2009**, *96*, 3331−3340.

(45) Popova, L. A.; Kodali, R.; Wetzel, R.; Lednev, I. K. Structural Variations in the Cross-β Core of Amyloid β Fibrils Revealed by Deep UV Resonance Raman Spectroscopy. *J. Am. Chem. Soc.* **2010**, *132*, 6324−6328.

(46) Asher, S. A.; Ianoul, A.; Mix, G.; Boyden, M. N.; Karnoup, A.; Diem, M.; Schweitzer-Stenner, R. Dihedral ψ Angle Dependence of the Amide III Vibration: A Uniquely Sensitive UV Resonance Raman Secondary Structural Probe. *J. Am. Chem. Soc.* **2001**, *123*, 11775−11781.

(47) Mikhonin, A. V.; Bykov, S. V.; Myshakina, N. S.; Asher, S. A. Peptide Secondary Structure Folding Reaction Coordinate: Correlation between UV Raman Amide III Frequency, ψ Ramachandran Angle, And Hydrogen Bonding. *J. Phys. Chem. B* **2006**, *110*, 1928−1943.

(48) Siamwiza, M. N.; Lord, R. C.; Chen, M. C.; Takamatsu, T.; Harada, I.; Matsuura, H.; Shimanouchi, T. Interpretation of the Doublet At 850 and 830 cm^{-1} in the Raman Spectra of Tyrosyl Residues in Proteins and Certain Model Compounds. *Biochemistry* **1975**, *14*, 4870−4876.

(49) Wang, Y.; Petty, S.; Trojanowski, A.; Knee, K.; Goulet, D.; Mukerji, I.; King, J. Formation of Amyloid Fibrils in Vitro from Partially Unfolded Intermediates of Human γC-Crystallin. *Invest. Ophthalmol. Visual Sci.* **2010**, *51*, 672−678.

(50) Chen, M. C.; Lord, R. C.; Mendelsohn, R. Laser-Excited Raman Spectroscopy Of Biomolecules IV. Thermal Denaturation of Aqueous Lysozyme. *Biochim. Biophys. Acta* **1973**, *328*, 252−260.

(51) Miura, T.; Takeuchi, H.; Harada, I. Characterization of Individual Tryptophan Side Chains in Proteins Using Raman Spectroscopy and Hydrogen-Deuterium Exchange Kinetics. *Biochemistry* **1988**, *27*, 88−94.

(52) Li, T.; Chen, Z.; Johnson, J. E.; Thomas, G. J., Jr. Structural Studies of Bean Pod Mottle Virus, Capsid, And RNA in Crystal and Solution States by Laser Raman Spectroscopy. *Biochemistry* **1990**, *29*, 5018−5026.

(53) Bhattacharya, M.; Jain, N.; Mukhopadhyay, S. Insights into the Mechanism of Aggregation and Fibril Formation from Bovine Serum Albumin. *J. Phys. Chem. B* **2011**, *115*, 4195−4205.